

## Strain-based fatigue reliability assessment of an automobile's lower arm for various road load conditions due to limited experimental data

Muhammad Ashraf Adam, Salvinder Singh Karam Singh\*, Shahrum Abdullah & Muhamad Alias Md. Jedi

*Department of Mechanical and Manufacturing Engineering,  
 Faculty of Engineering & Built Environment, Universiti Kebangsaan Malaysia, Malaysia  
 43600 UKM, 43600 Bangi, Selangor*

\*Corresponding author: [salvinder@ukm.edu.my](mailto:salvinder@ukm.edu.my)

Received 27 December 2023, Received in revised form 24 July 2024  
 Accepted 24 August 2024, Available online 30 January 2025

### ABSTRACT

*The aim of this paper is to characterise the strain-based fatigue reliability of a lower arm suspension system using strain signals captured from different types of road load conditions. Given the challenges of acquiring comprehensive loading history data and the inherent difficulties in capturing accurate load-time history data through laboratory or field-testing, a stochastic modelling approach was developed. Strain loads obtained from strain gauges were stochastically induced to generate random loads, which were then used to assess fatigue reliability based on the experimental data. The fatigue life, ranging from  $3.43 \times 10^5$  -  $9.02 \times 10^5$  cycles per block for highway, rural, and campus roads, was evaluated using the rainflow cycle counting technique through the strain life models, i.e. Coffin-Manson, Morrow, and Smith-Watson-Topper. Furthermore, the reliability of the induced fatigue life data was modelled using a Weibull distribution, resulting in a mean cycle to failure for the lower arm falling within the range of  $1.92 \times 10^6$  to  $2.53 \times 10^6$  cycles per block. Among the various road conditions analyzed, the highway exhibited the highest fatigue life, indicating that it is less prone to failure compared to other road conditions, which can be attributed to the smoother road profile. Hence, the use of stochastically induced random loads is proposed as an effective method for assessing strain-based fatigue reliability in aiding for the prediction of the durability and structural integrity of the lower arm suspension system.*

*Keywords: Fatigue reliability; strain life; durability; limited data; lower arm*

## INTRODUCTION

Fatigue reliability refers to assessing the probability of failure due to fatigue during the expected service life of a component or structure. Fatigue failure occurs when a material or structure undergoes repeated loading and unloading cycles, leading to the progressive accumulation of damage and eventual failure, even if the applied stresses are below the material's ultimate strength. In automobile reliability research, vehicles of different weights necessitate distinct tests for their components, resulting in varying strengths and levels of fatigue life (Soares et al. 2018). Furthermore, the amount of loading varies based on the types of roads used by the vehicles, as different roads exert varying amounts of stress on the parts (Putra, Husaini, and

Ikkal 2021). Suspension components, such as wheel rims and brake components, constitute unsprung masses. Therefore, reducing their weight is critical for ride quality, response, and overall vehicle weight reduction (Izzat et al. 2022). Several research studies focus on the suspension arm, including the dynamic assessment of motor vehicle suspension systems using the formulation of point-joint coordinates. The mechanical system is replaced with an equivalent system of constrained particles, and the equations of motion are derived using the principles of particle dynamics (Pachapuri et al. 2021). Consequently, to predict the fatigue life of a lower arm of the vehicle, a fatigue life assessment is established and proposed.

Strain-life models find application in fatigue analysis for predicting the fatigue life of materials or components based on the applied strain levels (Li and Chelidze 2021).

These models establish a correlation between cyclic strain amplitudes and anticipated fatigue life, providing estimates of the cycles a material can endure before experiencing failure. Commonly used models include Coffin-Manson, Morrow, and Smith-Watson-Topper (Kahoul et al. 2019). By delineating the relationship between strain and fatigue life, it becomes possible to assess durability, optimize designs, and ensure fatigue reliability in the lower arm. Strain-life models find extensive usage in various industries, including automotive, aerospace, and structural engineering, to evaluate the fatigue life of components and structures under cyclic loading conditions (B. J. Wang et al. 2020). Stochastic approaches, such as the Monte Carlo method, are employed in fatigue life analysis to incorporate randomness and probabilistic considerations (Karolczuk and Kurek 2022). The Monte Carlo method involves generating random samples based on probability distributions for input variables, such as stress amplitudes, and utilizing these samples for fatigue life assessment. Through repetitive simulation of fatigue life calculations using different input samples, statistical analysis can be conducted to estimate mean fatigue life, confidence intervals, and probability distributions (Ptak and Czmochowski 2023). The Monte Carlo method enables a comprehensive evaluation of fatigue performance, taking into account the variability and uncertainties associated with material properties, load conditions, and environmental effects. It facilitates the quantification of the probability of failure and aids in making informed decisions regarding design optimization and maintenance planning, thereby enhancing the reliability and durability of components and structures.

This study aims to model strain-based load–time history as an input from the Monte Carlo technique to predict accurately the fatigue reliability. Prior studies indicated that the road condition of less bump will have a longer fatigue reliability assessment, hence, least expected to fail based on the parameters used. This circumstance is due to the given constraints such as the design complexity and the sensitivity of the strain gauges that leads towards issues of missing data under operating conditions. Thus far, studies on the use of the probabilistic techniques in predicting the fatigue reliability of an automotive suspension remain limited. Thus, the stochastic approach of Monte Carlo is proposed to numerically induce random load–time history data by embedding experimentally captured stain-based loads for fatigue reliability prediction to improve the structural integrity of the component.

### METHODOLOGY

This study proposes a stochastic technique employing a probabilistic approach to generate random stress loading

history data under operating conditions, as illustrated in Figure 1. Strain-based loads are experimentally recorded at the critical region based on finite element analysis. Moreover, these recorded strain-based loads are stochastically induced to simulate random loads, allowing for the prediction of strain life using the rainflow cycle counting technique. Reliability analysis facilitates a comprehensive understanding of the suspension’s complete failure processes by considering the strain life under the impact of random loads and employing an appropriate distribution function.

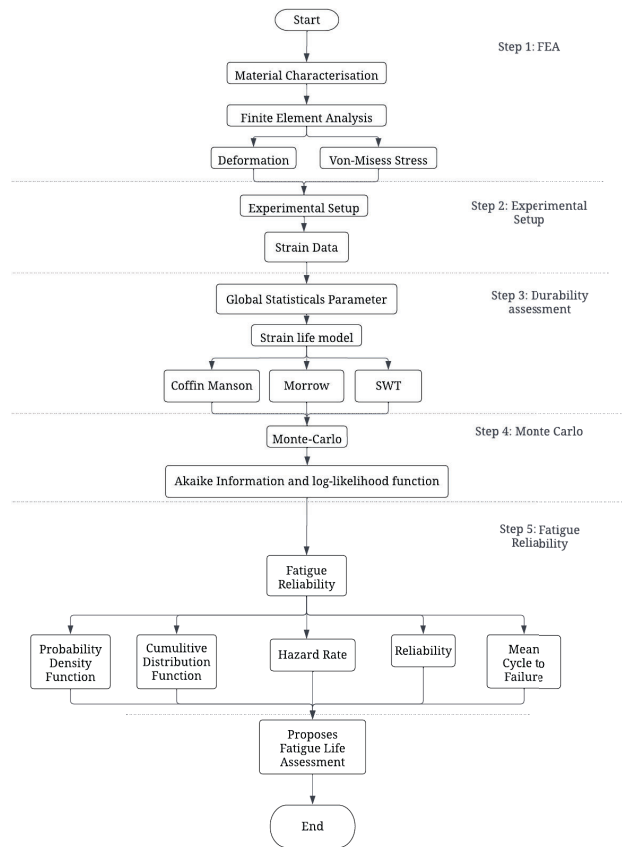


FIGURE 1. Flow process of the analysis

### MATERIAL CHARACTERISATION

In the process of material characterization, the lower arm of the car materials was SAE 1045. To effectively characterize these materials, a tensile test was performed to determine the ultimate tensile strength, ensuring the reliability and usability of the obtained data (Dominguez Almaraz, Ruiz Vilchez, and Dominguez 2019).

For the tensile test, a standard ASTM E8-11 sample was selected for conducting the experiment, with the specimen size based on the specifications outlined in Figure 2.

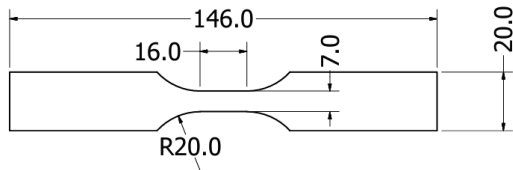


FIGURE 2. ASTM E8-11 sample used for tensile test

For additional material characterization, a sample of the failed lower arm was extracted and sent for field emission scanning electron microscopy (FE-SEM) analysis. The aim was to capture the microstructure image of the materials, identify the specific material components, and examine the cross-section where the failure took place in the lower arm. (Bodik et al. 2022)(Cristina et al. 2023).

### CRITICAL LOCATION ASSESSMENT

The mesh, the boundary condition, and the load applied are shown in Figure. 1. The SAE 1045 carbon steel material was utilised in FEA as a lower arm is commonly made a carbon steel of SAE 1045 (Dominguez Almaraz, Ruiz Vilchez, and Dominguez 2019). The mechanical properties for SAE 1045 carbon steel are as follows: the ultimate tensile strength,  $S_u$  of 565 MPa, a yield strength,  $S_y$  is 310 MPa, a modulus of elasticity,  $E$  is 206 GPa, and Poisson ratio is 0.29. In this study, the mesh size of 2 mm with 62300 elements and 116359 nodes with a curb weight of

1017 kg with a quarter load of 2.04 kN as shown in Figure 3.(Souiyah 2021) (Amir et al. 2020)

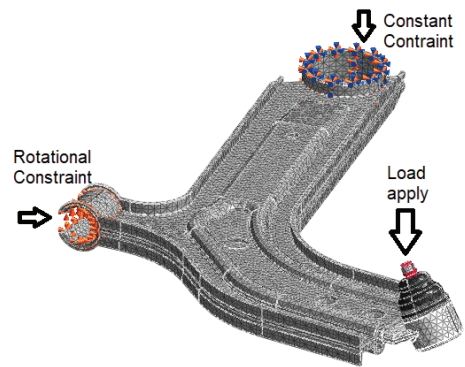


FIGURE 3. Load applied and boundary condition of the lower arm based on the quarter car model

### EXPERIMENTAL SETUP AND GLOBAL STATISTICAL ANALYSIS

The strain time-series history data were experimentally captured at the sampling rate of 500 Hz for 60 s from three different road conditions, i.e., highway roads, campus roads, and rural roads (Putra, Husaini, and Machmud 2020). The strain gauge of 1 mm was positioned on the lower arm hotspot based on the critical region obtained from the finite elements analysis as shown in Figure 4.

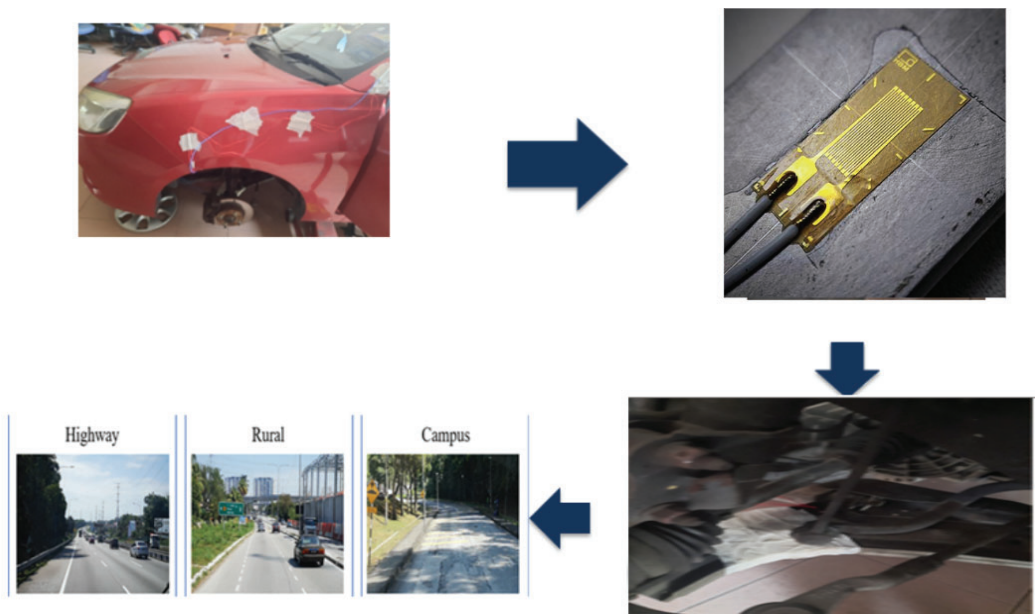


FIGURE 4. Experiment setup to capture strain data for various load condition

From the captured data, the global statistics were extracted to characterise the feature of the data through the mean, standard deviation, kurtosis, root-mean-square, and power spectrum density (Q. Wang et al. 2021)(Zhang, Lv, and Ge 2021). The mean of a strain signal is a measure of its central tendency and represents the average value of the strain data points. The mean value  $\bar{x}$  of the signal was calculated by using the formula below:

$$\bar{x} = \frac{1}{n} \sum_{j=1}^n F \quad (1)$$

The standard deviation (SD) measure of the dispersion or variability of the strain signal. It quantifies how the strain values deviate from the mean., and is shown as below:

$$SD = \sqrt{\frac{1}{n} \sum_{j=1}^n (F - \bar{x})^2} \quad (2)$$

The root-mean square (RMS) measure of the overall magnitude or amplitude of the strain signal. It is shown as below:

$$r. m. s. = \left( \frac{1}{2} \sum_{i=1}^n F_i^2 \right)^{\frac{1}{2}} \quad (3)$$

Kurtosis is a statistical statistical measure that describes the shape of the distribution of a dataset, specifically its tail behavior. It indicates whether the data has heavy or light tails compared to a normal distribution by using the formula below:

$$K = (n^{-1}SD^{-4}) \sum_{i=1}^n (F_i - \bar{x})^4 \quad (4)$$

These formulas provide a basic understanding of how to calculate the mean, standard deviation, root-mean-square (RMS), and kurtosis from a strain signal.

## STRAIN-BASED FATIGUE LIFE ASSESSMENT

The suspension is subjected to random stress time history loads that influences the number of cycles to failure. Hence, the rainflow cycle counting rainflow cycle technique is proposed as it pairs the localised minima and maxima to calculate an equivalent cycle with the smallest standard deviation (Pham et al. 2021; Fu et al. 2020). The result will provide an excursion downwards or upwards within the

given maximum and minimum interval range in order to assess the linear fatigue damage concerning the durability of the components as by the fatigue life of the structure under that specific load based on Equation 1.

$$D = \sum(N_i/N_f) \quad (5)$$

Where  $D$  is the total accumulated damage,  $N_i$  is the number of cycles for the  $i$ th load history, and  $N_f$  is the fatigue life of the structure under that specific load history. The linear cumulative damage rule assumes that the fatigue life under each load history is independent and that the damage caused by each load history is linearly additive. The fatigue life was based on the Coffin-Manson, Morrow, and Smith Watson-Topper (SWT) strain life model as shown in Equation (6-8) (Q. Wang et al. 2021)(H. Wang, Xuan, and Liu 2021):

Coffin Manson: - which does not consider the effect of mean stress based on damage value

$$\varepsilon = \frac{\sigma'_f}{E} (2N_f)^b + \varepsilon'_f (2N_f)^c \quad (6)$$

where  $\varepsilon$  is the strain amplitude,  $\sigma'_f$  is the fatigue strength coefficient,  $E$  is the material modulus of elasticity,  $N_f$  is the number of cycles to failure for a particular stress range and mean,  $b$  is the fatigue strength exponent,  $\varepsilon'_f$  is the fatigue ductility coefficient, and  $c$  is the fatigue ductility exponent (L. Abdullah et al. 2021).

In addition, the Morrow and Smith-Watson-Topper as shown in Equation (7) and (8) assesses the deterioration of the components' life due to the cyclic strain range under operating conditions, the total strain amplitudes, compressive stress and maximum tensile stress for uniaxial loading. Hence, these models consider the effects of mean stress on fatigue behaviour

$$\varepsilon = \frac{\sigma'_f - \sigma_{mean}}{E} (2N_f)^b + \varepsilon'_f (2N_f)^c \quad (7)$$

:

$$\sigma_{max} \varepsilon = \frac{\sigma'_f{}^2}{E} (2N_f)^{2b} + \varepsilon'_f (2N_f)^{b+c} \quad (8)$$

where  $E = 206$  GPa which is the material elastic modulus for the SAE 1045;

## STRAIN-BASED FATIGUE RELIABILITY ASSESSMENT

In order to assess the strain-based fatigue reliability from the life data, the selection of the suitable density function is important as it will affect the accuracy of the applied statistical model. Several distribution models are widely employed for fatigue analysis, such as the Gaussian (Tognan and Salvati 2023), Weibull (Sarkar et al. 2019), and Gumbel (Nagode et al. 2023) distributions. The reliability analysis is important in characterising the life data of the captured strain data from the suspension under operating loads in relation to cumulative fatigue damage. The statistical moments of the captured strain time-series data i.e. standard deviation, skewness, kurtosis and mean are used to illustrate the characteristics of fatigue life data from the Weibull distribution as mentioned in Eq 9 (Molina, Piña-Monarez, and Barraza-Contreras 2020).

$$f(N_f) = \frac{\beta}{\theta} \left(\frac{N_f}{\theta}\right)^{\beta-1} e^{-\left(\frac{N_f}{\theta}\right)^\beta} \quad (9)$$

where  $\theta$  and  $\beta$  are the characteristic scale parameter and shape parameter (Strzelecki 2021).

The random strain-based loads will affect the durability of the suspension and can be related directly to the failure behaviour of the components in terms of early, constant or end of service life failures through the estimated  $\beta$  range. The changes of  $\beta$  is associated the distribution curve of the operating strain load history for the suspension (Kahoul et al. 2019). The desired reliability life–safe life of the crankshaft for the  $N_f$  can be evaluated as:

$$f(N_f) = 1 - \exp\left(-\left(\frac{\theta}{N_f}\right)^\beta\right) \quad (10)$$

where  $\beta$  is the shape parameter,  $\theta$  is the scale parameter and  $N_f$  is the number of cycles to failure based on the strain loading histories.

The captured random strain loads are the structural response from the suspension under operating condition that related towards hazard rate of the component. Therefore, strain time-series load history will determine failure characteristics (Singh, Abdullah, and Ariffin 2020):

$$f(N_f) = \frac{\beta}{\theta} \left(\frac{N_f}{\theta}\right)^{\beta-1} \quad (11)$$

Likewise, the mean cycle to failure MCTF based on the  $N_f$  that be used to represent the specified cycle can be illustrated as (Nasir et al. 2020):

$$MCTF = \mu - 0.5776\beta \quad (12)$$

Where  $\beta$  is the scale,  $\mu$  is the parameter of location and Euler's constant is 0.5776.

## RESULTS AND DISCUSSION

### FAILURE CHARACTERISATION

In the conducted tensile test, the ultimate tensile strength was determined to be 676 MPa, with a yield point at 376 MPa and an elastic modulus of 208 GPa. These experimental values were used as a reference point for comparison with the preset data. The results of the tensile test are illustrated in Figure 5.

The findings from the FE-SEM analysis revealed the material composition, along with a detailed view of the cross-section of the failed lower arm. Figure 6 displays the cross-section of the lower arm, illustrating the area where the failure occurred (Welch-Phillips et al. 2020).

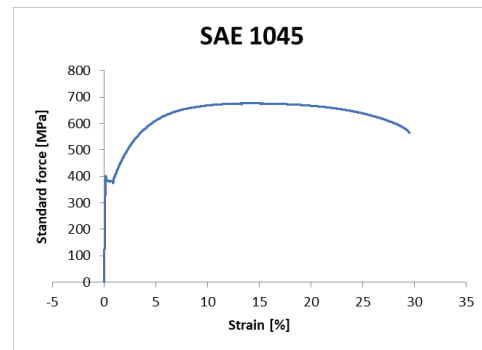


FIGURE 5. Tensile test results



FIGURE 6. Cross-sectional of lower arm

For the EDX of the material it is shown in Figure 7 that the material for the lower arm is mainly consists of

carbon followed by zinc, iron, silicon and aluminium (Cristina et al. 2023) (Monedero-Contreras, Martínez-Ruiz, and Rodríguez-Tovar 2023).

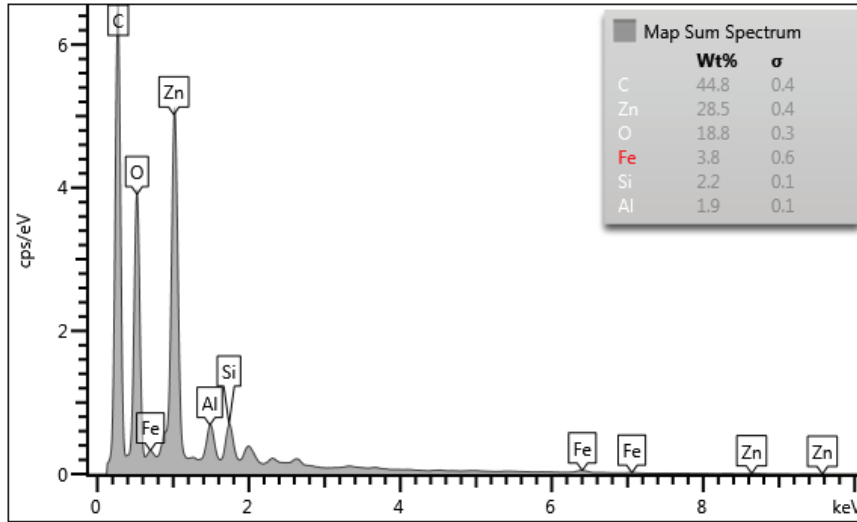


FIGURE 7. EDX of the lower arm

STRESS CONVERGENCE

In order to determine the convergence of the von-Mises stress, various mesh sizes from 2 mm to 10 mm were modelled. From Figure 8, it is observed that it converged at 2 mm (Alias, Matlan, and Kasa 2020). Finite element was conducted to determine a hotspot or critical contour on a model of automotive component with a load of 2.04 kN based on the quarter car model (Patil and Jadhav 2020).

The maximum deformation was shown at 15 mm at bulk of the lower arm area as displayed in Figure 9(a). However, the von-Mises stress concentration achieved 2.1 MPa at the critical contour, as illustrated in Figure 9(b). This result was used to determine the location to fixed a strain gauge. The maximum von-Mises was obtained at 2.1 MPa, where it was found to be lesser than the ultimate tensile strength of 676 MPa. As a result, this is applicable to determine the hotspot or critical region.

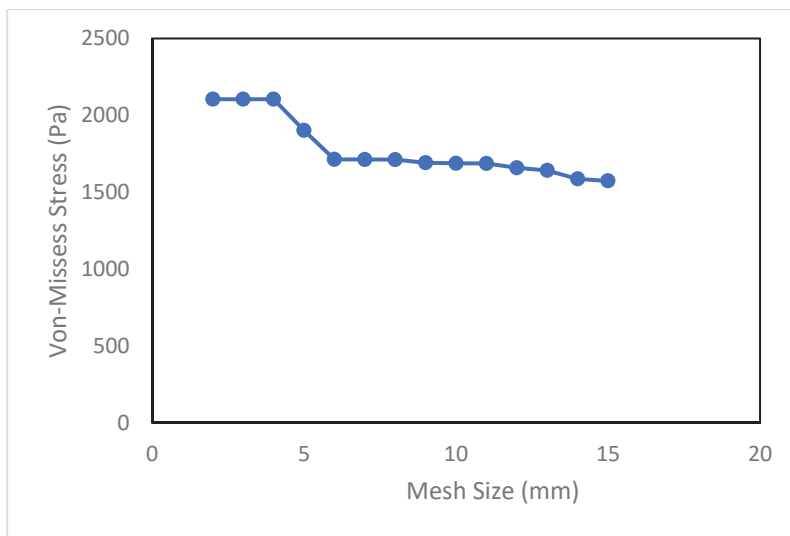
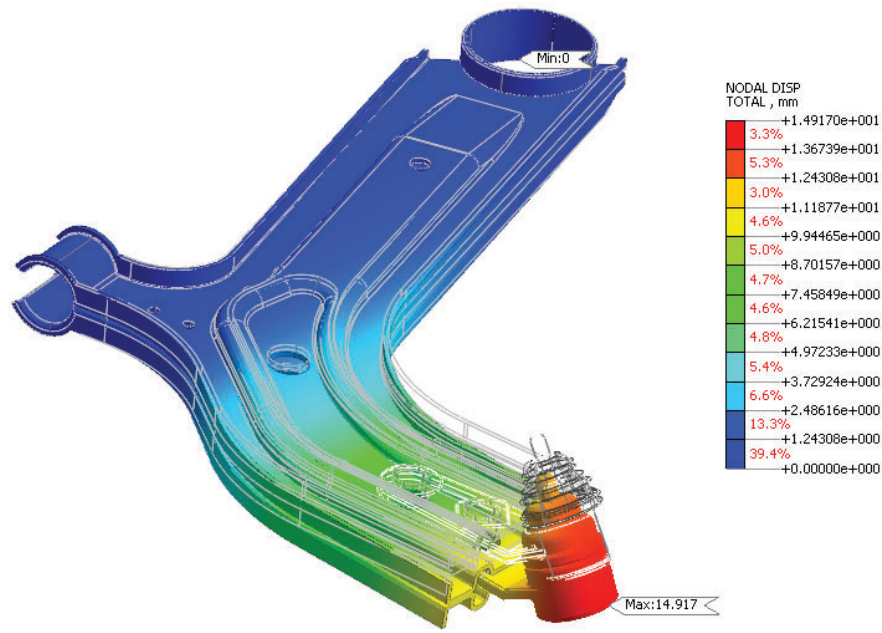
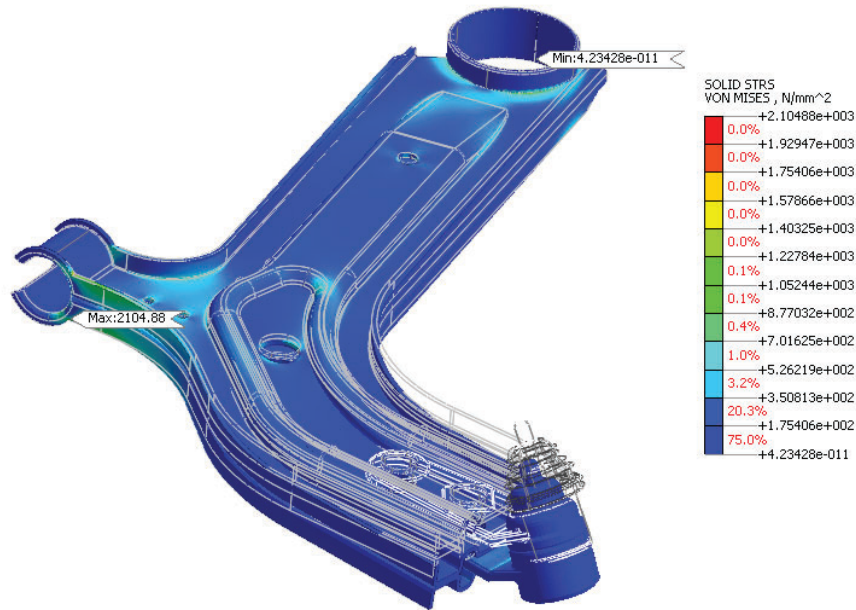


FIGURE 8. Stress convergence of the lower arm



(a)



(b)

FIGURE 9. (a) dan (b) shows the deformation and Von-Misses Stress of the lower arm

STATISTICAL ASSESSMENT FROM THE CAPTURED STRAIN TIME-SERIES HISTORY

Figure 10 displays the strain-based time history for the three-road condition which involves highway, rural dan

campus data at a sampling rate of 500Hz for 60 seconds. This frequency is appropriate for on-site data collection given that sampling frequencies for signal loading measurements should be greater than 400 Hz (Abd Rahim et al. 2019). This is because fatigue damage occurs at lower frequencies (H. Wang, Xuan, and Liu 2021).

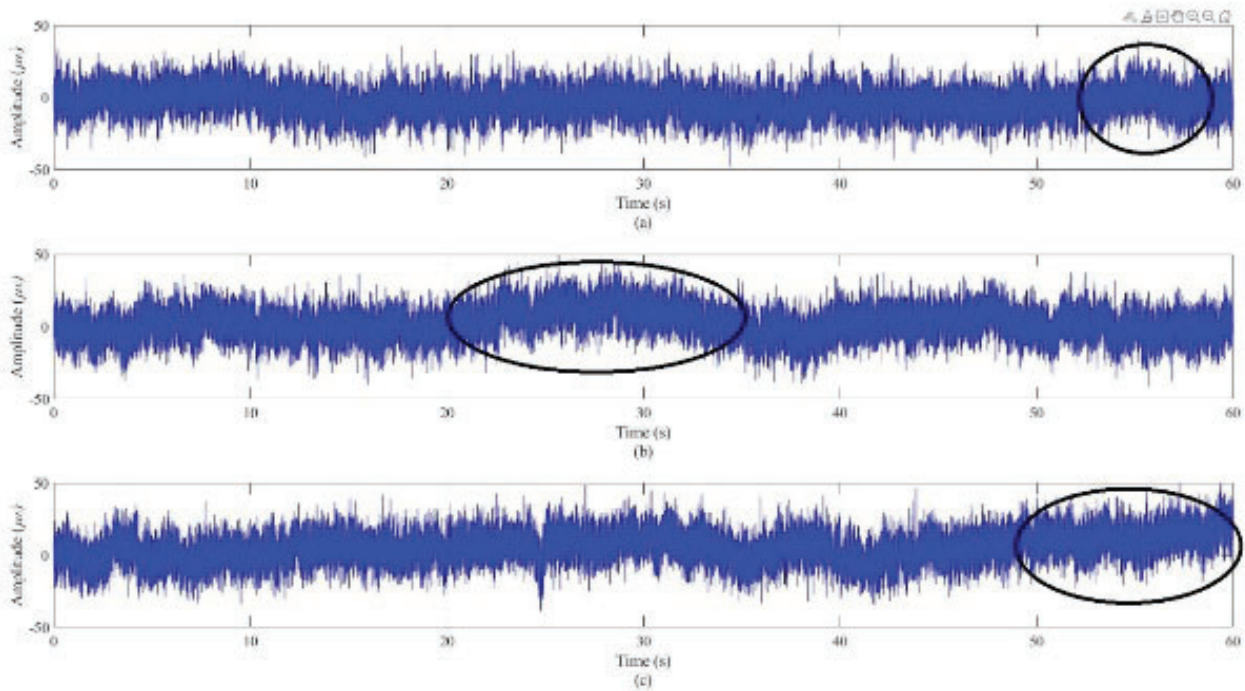


FIGURE 10. Strain signal from (a) highway roads, (b) campus roads, and (c) rural roads

The statistical characteristics for each signal are tabulated in Table 1 based on the mean ( $\mu$ ), standard deviation ( $\sigma$ ), kurtosis (K), and root mean square (RMS). In addition, the parameters used to characterise the strain signals when analysing random loading data were based on the energy (RMS) and kurtosis associated with the state of the roads (Nasir et al. 2020). In comparison towards signals captured from the various roads, the RMS for rural

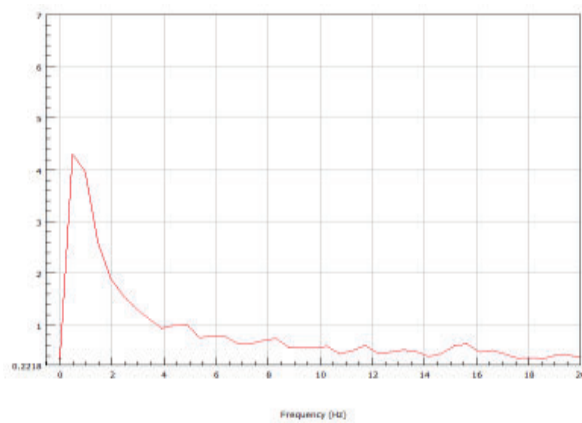
roads had the highest value at 11.4. This is due to road profile, it has been observed there were multiple amplitude range, which could have affected the suspension rather than in the highway and campus data (Lennie Abdullah et al. 2020). In contrast to the results for the campus and highway data, the kurtosis value for the rural data was the lowest. This might be due to low-amplitude occurrences happening on unpaved rural roads.

TABLE 1. Characterisation of Signal

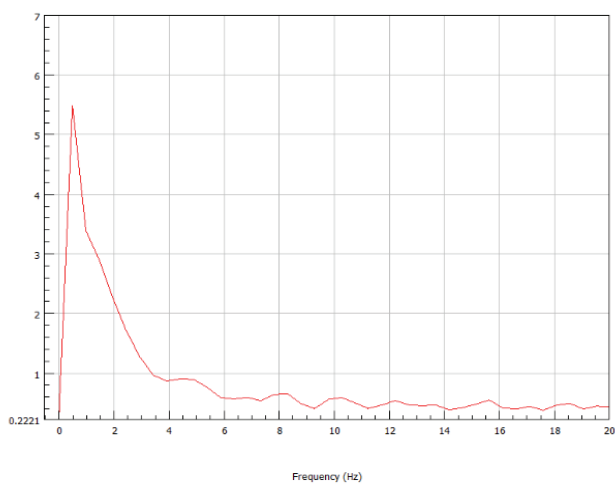
Characterisation of Signal	Type of Road		
	Highway	Campus	Rural
$\mu$	-3.23	5.25	11.2
$\sigma$	10.4	11.3	2.26
K	10.9	12.5	3.02
RMS	3.01	2.92	11.4

The power spectral density (PSD) (González, Feng, and Casero 2023) for each of the three signals is shown in Figure 11. The PSD obtained from highway road demonstrated to be the lowest among the rural and campus

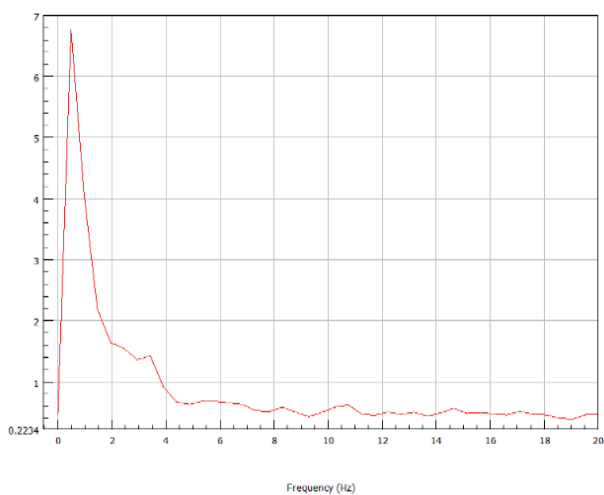
roads at 4.3 due to the highway roads is smoother and less bumpy compare to the campus and rural roads thus the value will be the lowest among the three roads.



(a) Highway



(b) Campus



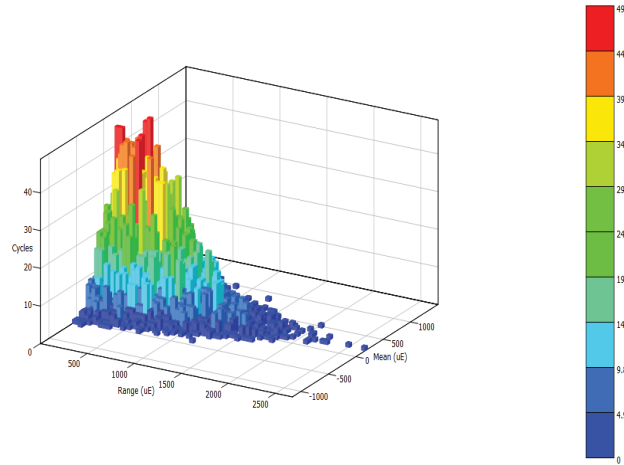
(c) Rural

FIGURE 11. Power spectral density (PSD) from (a) highway roads, (b) campus roads, (c) rural roads, and (d) combined roads

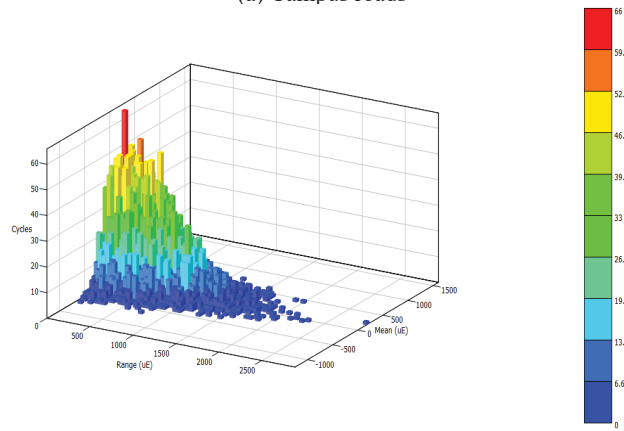
## STRAIN-BASED FATIGUE LIFE ASSESSMENT

Figure 12 depicts the rainflow histogram of the three roads' conditions, which was used to begin evaluating the three roads' durability by determining a cycle amplitude from the data on variable amplitude strain loads using the rainflow counting method (Kebir et al. 2020). It was used

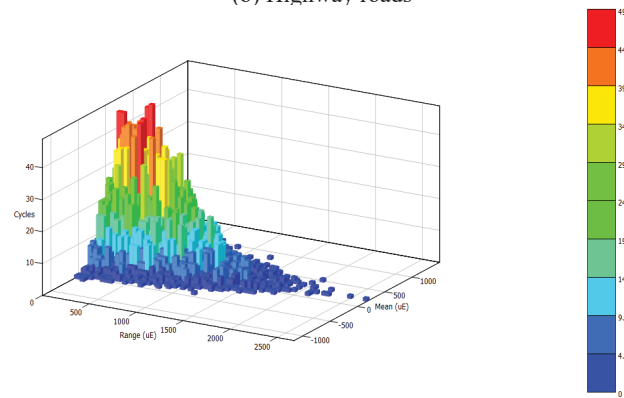
to calculate damage by comparing the average values of the stress cycle and amplitude. In contrast to campus and rural data shows a substantial dispersion on highway data at a lower cycle range. As opposed to highway data, where a low amplitude range was obtained while the vehicle was in a braking condition, campus and rural data primarily featured low amplitude ranges (Pham et al. 2021).



(a) Campus roads



(b) Highway roads



(c) Rural roads

FIGURE 12. Rainflow histogram for three roads.

From Table 2, the strain life model of Coffin-Manson model has a longer fatigue life than the Morrow and SWT models because the computation for the former model did not consider for the effects of mean stress. Accordingly, as for the Morrow and SWT model, the campus road data had the range of fatigue life at  $3.43 \times 10^5 - 5.97 \times 10^5$  cycles/block. Likewise, the rural data had a fatigue life of  $5.18 \times 10^5 - 6.3 \times 10^5$  cycles/block, while the highway data had

a fatigue life of  $6.93 \times 10^5 - 9.02 \times 10^5$  cycles/block. This because the Morrow and SWT models assesses the deterioration of the components' life due to the cyclic strain range under operating conditions, the total strain amplitudes, compressive stress and maximum tensile stress for uniaxial loading. Hence, providing the mean stress effect had a significant impact on fatigue life (Putra, Abdullah, and Schramm 2020).

TABLE 2. Life data obtained from strain signals

Strain-life model	Road type	Life value
Coffin-Manson	Highway	$6.93 \times 10^5$
	Campus	$5.97 \times 10^5$
	Rural	$6.56 \times 10^5$
Morrow	Highway	$7.74 \times 10^5$
	Campus	$5.12 \times 10^5$
	Rural	$6.30 \times 10^5$
SWT	Highway	$9.02 \times 10^5$
	Campus	$3.43 \times 10^5$
	Rural	$5.18 \times 10^5$

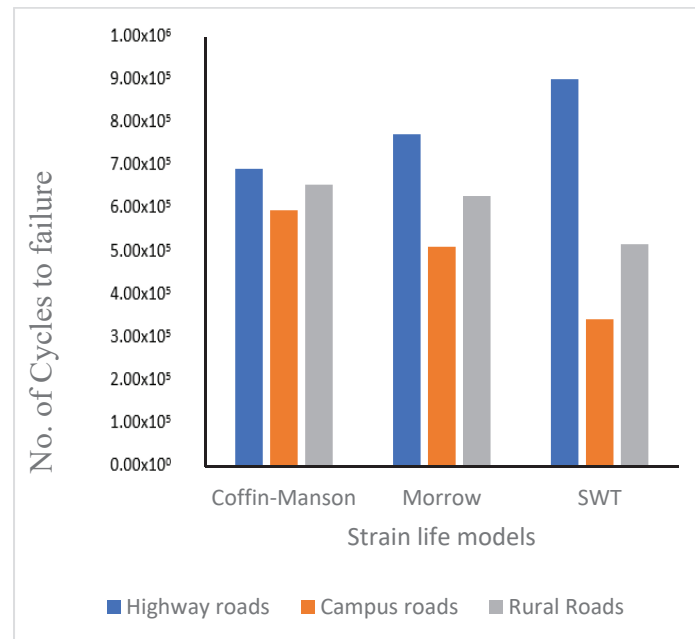


FIGURE 13. Fatigue life

In order to determine the appropriate distribution model in determining the fatigue reliability of the suspension, the log-likelihood (LL) and the Akaike's information criterion (AIC) is deployed for each strain life model are shown in Table 3. It illustrates that the Weibull distribution, followed by the Gaussian and Lognormal distributions, provided the highest result based on the LL

value (Molina, Piña-Monarez, and Barraza-Contreras 2020). The AIC value showed that the Weibull distribution yielded the least value of the three described distributions. Because the AIC values of the Gaussian and Lognormal distributions were greater than those of the Weibull distribution, the Weibull distribution was chosen based on the findings of this study (Park et al. 2023). Automotive

component mechanical failure and fatigue life were predicted using the Weibull distribution. As a result, one of the probabilistic models suited for analysing the random

variable data in this study was the Weibull distribution (Chin et al. 2021).

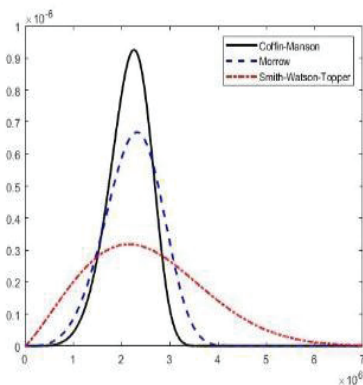
TABLE 3. Log-likelihood and Akaike’s information criterion values for all strain life models

Strain-Life Model	Distribution	Log Likelihood	AIC
Coffin-Manson	Lognormal	-36.15	78.3
	Weibull	-35.91	77.82
	Gaussian	-36.12	78.24
	Lognormal	-39.09	84.18
	Weibull	-39.02	84.04
Morrow	Gaussian	-39.11	84.22
	Lognormal	-41.2	88.4
	Weibull	-41.23	88.46
SWT	Gaussian	-41.45	88.9

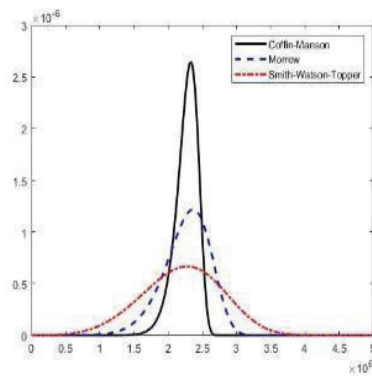
PROBABILISTIC FATIGUE RELIABILITY ASSESSMENT FROM THE STRAIN LIFE MODELS

Due to the limited strain-based life obtained from the experimental analysis, the Monte Carlo technique is proposed to be stochastically induced into the Weibull distribution function as shown in Figure. 14 for strain life model (Tsai and Alipour 2020). The Morrow and SWT models were tilted to the left, indicating that the lower arms would have a shorter fatigue life according to these models. This was owing to the compression and strain that the lower

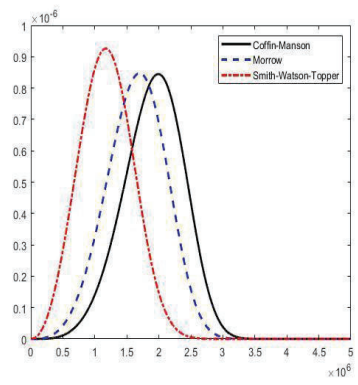
arms endured, which the SWT and Morrow models accounted for in their models (Rahim et al. 2021). The cumulative distribution function shown in Figure 15 indicated that the SWT model had a higher likelihood of failure than the Morrow and Coffin-Manson models. All the Coffin-Manson model, Morrow model, and SWT model had failure probabilities that fell within the range of 0.46 -0.53, 0.43-0.57, and 0.72-0.86, respectively. This indicates that the corresponding Coffin-Manson, Rural, and SWT models, lower arms may sustain damage at failure rates greater than 0.53, 0.57, and 0.86 (Nasir et al. 2020).



(a) Campus

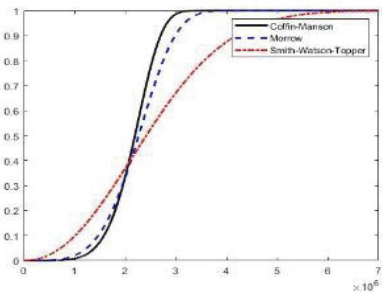


(b) Highway

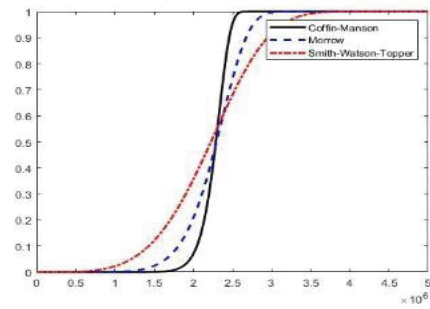


(c) Rural

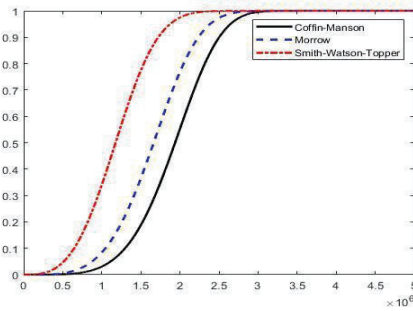
FIGURE 14. Strain-based fatigue life distribution for the various road condition



(a) Campus

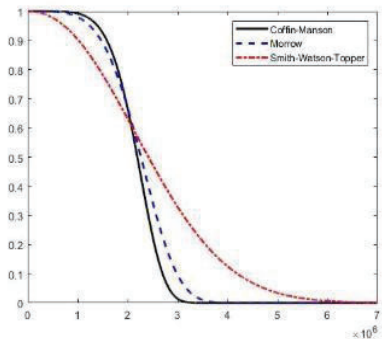


(b) Highway

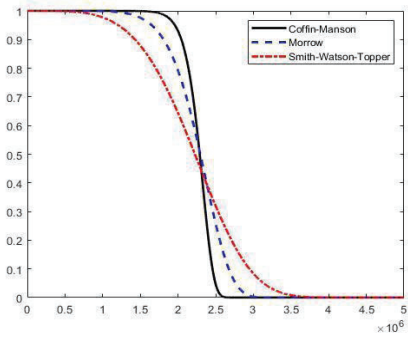


(c) Rural

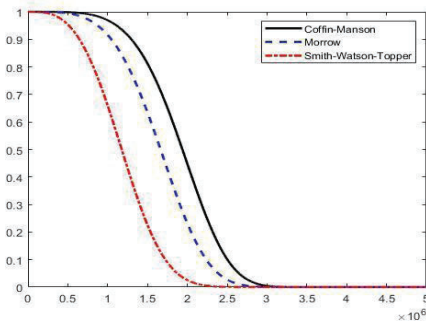
FIGURE 15. Strain-based fatigue life cumulative distribution for the various road condition



(a) Campus



(b) Highway



(c)

FIGURE 16. Strain-based fatigue life reliability for the various road condition

The reliability assessment for the reliability and hazard rate was based on fatigue life according to the road conditions, as depicted in Figure. 16, respectively. Unlike the Morrow and SWT models, the Coffin-Manson model did not account for the effects of mean stress. The tension-compression effect that resulted from the lower arm’s operating condition was the cause of the mean stress effect (Chin, Abdullah, et al. 2021). As a result, it was possible to perform the proposed fatigue life reliability assessment utilising life data derived from strain signals from various types of roads.

The campus road’s hazard rate for the SWT model was  $8.0 \times 10^5$  cycles/block, while the Coffin-Manson and Morrow models had rates of  $8.6 \times 10^5$  and  $3.7 \times 10^5$  cycles/block, as shown in figure 17 respectively. The hazard rate indicates that as the number of cycles rises, so does the hazard rate until damage is done (Kebir et al. 2020). The SWT model may take into account the mean stress effect, and a lower arm may suffer compression and tension frequently. The hazard rate of the McTF point was defined to be in the range of  $1.09 \times 10^{-5}$  to  $3.86 \times 10^{-6}$  cycles/block. As a result, the harm was displayed in a low hazard area.

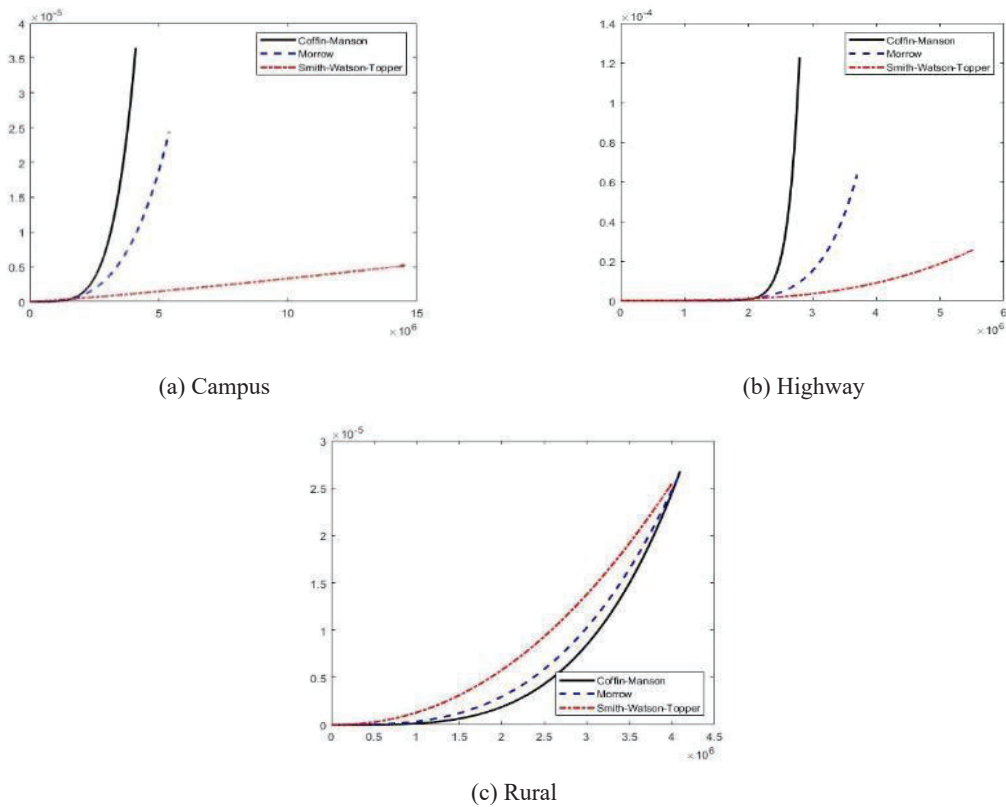


FIGURE 17. Strain-based fatigue life hazard curve for the various road condition

Figure. 18 depicts the mean cycle to failure (McTF), and this value was defined using the Weibull distribution’s mean. The results demonstrate that the Coffin-Manson, Morrow, and SWT models’ McTF values ranged from  $1.92 \times 10^6$ - $2.53 \times 10^6$  to  $1.65 \times 10^6$  to  $2.26 \times 10^6$  and  $1.18 \times 10^6$  to  $2.53 \times 10^6$  cycles/block, respectively (Molina, Piña-Monarez, and Barraza-Contreras 2020). In reliability and hazard rate graphs, these McTF values were utilised to determine where the value resided at the McTF point. In

addition to McTF, both the Coffin-Manson model and the SWT model provided the highest values for scale parameters, at 16.8 and 2.86 respectively. Due to the Coffin-Manson model’s exclusion of using mean stress in its computation, it offered the maximum value for the Weibull characteristics (Zang et al. 2024). It is suggested that the Weibull probability distribution be used to model the reliability evaluation connected to the fatigue life data.

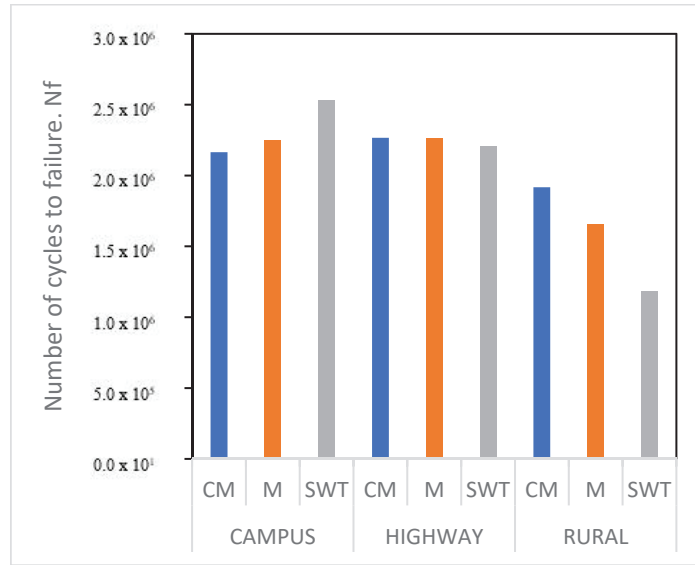


FIGURE 18. Mean cycle to failure for all strain life models

From Figure 10, the correlation of the mean cycle to failure (McTF) is scattered within a range of ( $10^5$ -  $10^6$ ) of the correlation line. The rural is above the correlation line for the McTF while the highway is within the correlation line while for campus the data is slightly below the correlation line. All the data points fit within the conventional fatigue life boundaries of 1:2 and 2:1 and shown in Figure 19 (Singh, Abdullah, and Ariffin 2020).

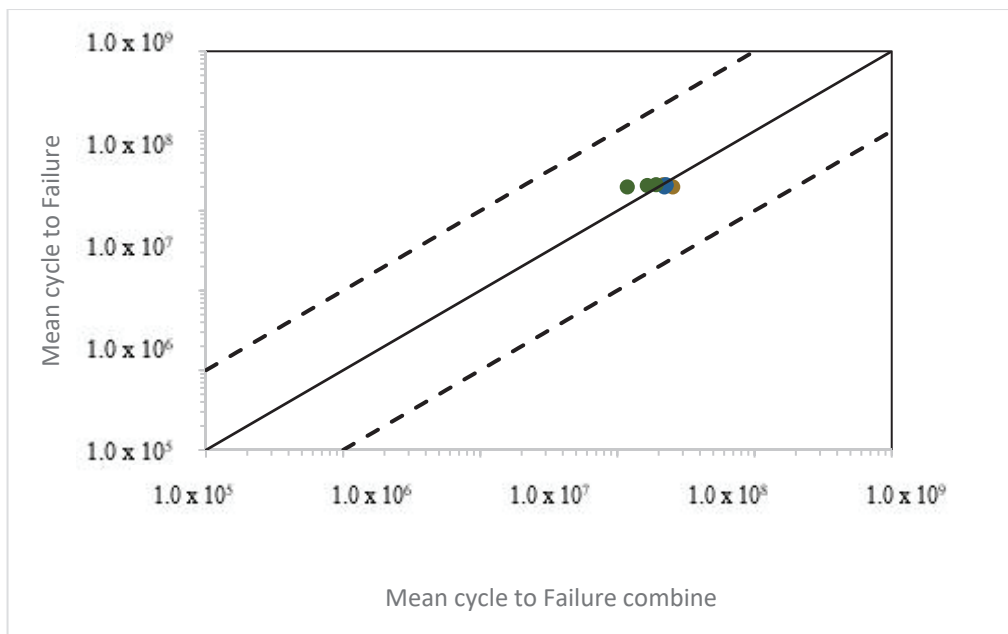


FIGURE 19. Correlation of McTF

### CONCLUSION

It can be concluded that the condition of highway roads demonstrated a significantly longer life compared to the other two road types, namely rural roads and campus roads.

This conclusion is drawn based on the analysis conducted using three different strain models, namely Coffin-Manson, Morrow, and SWT life strain models. The application of these strain models yielded distinct sets of life data, with the Coffin-Manson model producing the highest life data among the three. However, it should be noted that this

disparity in results could be attributed to the Coffin-Manson model's exclusion of mean stress in its calculation. Despite this discrepancy, the fatigue data for the highway roads consistently exhibited the highest values across all types of models, regardless of the road conditions.

The inputs of the strain-based fatigue life data, the fatigue reliability is modelled by extracting the features of only the high amplitude excitation obtained in time-domain strain signals. The Weibull distribution was selected based on the AIC values obtained from the fatigue life data generated by all strain life models. The distribution facilitated the determination of the McTF values, which were subsequently utilized for the data analysis of the PDF, CDF, reliability, and hazard rate of the fatigue life in relation to the different road types. Therefore, based on the findings of the proposed fatigue reliability assessment, it can be concluded that the Morrow and Smith-Watson-Topper model is proposed as the appropriate strain-life model due to the tension-compression effect that resulted from the lower arm's operating condition that was caused by the mean stress effect from the various road condition.

## ACKNOWLEDGEMENT

The authors would like to express their gratitude to Universiti Kebangsaan Malaysia (Research funding: GUP-2022-013 & FRGS/1/2023/TK10/UKM/02/1) for supporting this research.

## DECLARATION OF COMPETING INTEREST

None.

## REFERENCES

- Abd Rahim, Airee Afiq, Shahrum Abdullah, Salvinder Singh Karam Singh, and Mohd Zaki Nuawi. 2019. Reliability assessment on automobile suspension system using wavelet analysis. *International Journal of Structural Integrity* 10 (5): 602–11. <https://doi.org/10.1108/IJSI-04-2019-0035>.
- Abdullah, L., S. S.K. Singh, S. Abdullah, A. H. Azman, and A. K. Ariffin. 2021. Fatigue reliability and hazard assessment of road load strain data for determining the fatigue life characteristics. *Engineering Failure Analysis* 123 (December 2020): 105314. <https://doi.org/10.1016/j.engfailanal.2021.105314>.
- Abdullah, Lennie, Salvinder Singh Karam Singh, Shahrum Abdullah, Abdul Hadi Azman, Ahmad Kamal Ariffin, and Yat Sheng Kong. 2020. The needs of power spectral density in fatigue life prediction of heavy vehicle leaf spring. *Journal of Mechanical Science and Technology* 34 (6): 2341–46. <https://doi.org/10.1007/s12206-020-0510-z>.
- Alias, Rohaya, Siti Jahara Matlan, and Anuar Kasa. 2020. Finite element performance with different mesh size of retaining walls. *International Journal of Advanced Research in Engineering and Technology* 11 (3): 381–89. <https://doi.org/10.34218/IJARET.11.3.2020.033>.
- Amir, Mohd, Shazwan Hashim, Balaji P Muthaiyah, Shaheerthana Suresh, Muhammad Izzat, Nor Ma'arof, and Girma Tadesse Chala. 2020. Finite element analysis of a buggy car's suspension arms for off-road usage 2020 (September): 23. <http://eprints.intimal.edu.my/1438/>.
- Bodik, Michal, Christopher Walker, Maksym Demydenko, Thomas Michlmayr, Thomas Bähler, Urs Ramsperger, Ann Katrin Thamm, et al. 2022. The effect of work function during electron spectroscopy measurements in scanning field-emission microscopy. *Ultramicroscopy* 238 (March). <https://doi.org/10.1016/j.ultramic.2022.113547>.
- Chin, C. H., S. Abdullah, S. S.K. Singh, D. Schramm, and A. K. Ariffin. 2021. Durability prediction of coil spring through multibody-dynamics-based strain generation. *Mechanical Systems and Signal Processing* 154: 107580. <https://doi.org/10.1016/j.ymsp.2020.107580>.
- Chin, C. H., A. A.A. Rahim, S. Abdullah, S. S.K. Singh, and N. Md Nor. 2021. Acceptability of the effective strain damage model for fatigue life assessment considering the load sequence effect for automotive coil spring. *Engineering Failure Analysis* 126 (December 2020): 105462. <https://doi.org/10.1016/j.engfailanal.2021.105462>.
- Cristina, Maria, Giuseppe Fierro, Aidan M Doyle, Simonetta Tuti, Carlotta Catracchia, and Daniela Pietrogiamici. 2023. combined use of in situ and operando- FTIR , TPR and FESEM techniques to investigate the surface species along the simultaneous abatement of N<sub>2</sub> O and NO on Pt , Pd , Rh / TiO<sub>2</sub> -ZrO<sub>2</sub> and Pt , Pd , Rh / TiO<sub>2</sub> -ZrO<sub>2</sub> -CeO<sub>2</sub> catalysts. 42 (July). <https://doi.org/10.1016/j.surfin.2023.103502>.
- Dominguez Almaraz, G. M., J. A. Ruiz Vilchez, and Alexiane Dominguez. 2019. Ultrasonic fatigue on the automotive steels: AISI/SAE 4140T and 1045. *Procedia Structural Integrity* 18: 594–99. <https://doi.org/10.1016/j.prostr.2019.08.204>.
- Fu, Bing, Jianbin Zhao, Bingqing Li, Jing Yao, Armand Robinson Mouafo Teifouet, Liyun Sun, and Zhenyu Wang. 2020. Fatigue reliability analysis of wind turbine tower under random wind load. *Structural Safety* 87 (April 2019): 101982. <https://doi.org/10.1016/j.strusafe.2020.101982>.

- González, Arturo, Kun Feng, and Miguel Casero. 2023. Effective separation of vehicle, road and bridge information from drive-by acceleration data via the power spectral density resulting from crossings at various speeds. *Developments in the Built Environment* 14 (April). <https://doi.org/10.1016/j.dibe.2023.100162>.
- Izzat, Muhammad, Nor Ma, G K H Tan, K H Lim, and G T Chala. 2022. Assessment of FSAE car's rear suspension arms for bump force. (21): 1–6.
- Kahoul, Hafida, Samira Belhour, Ahmed Bellaouar, and Jean Paul Dron. 2019. Fatigue life prediction of upper arm suspension using strain life approach. *Journal of Engineering, Design and Technology* 17 (1): 25–40. <https://doi.org/10.1108/JEDT-03-2018-0047>.
- Karolczuk, Aleksander, and Marta Kurek. 2022. Fatigue life uncertainty prediction using the monte carlo and latin hypercube sampling techniques under uniaxial and multiaxial cyclic loading. *International Journal of Fatigue* 160 (March): 106867. <https://doi.org/10.1016/j.ijfatigue.2022.106867>.
- Kebir, Tayeb, José A.F.O. Correia, Mohamed Benguediab, and Abilio M.P.De Jesus. 2020. Numerical study of fatigue damage under random loading using rainflow cycle counting. *International Journal of Structural Integrity* 12 (3): 408–18. <https://doi.org/10.1108/IJSI-04-2020-0036>.
- Li, He Wen Xuan, and David Chelidze. 2021. Fatigue life estimation of structures under statistically and spectrally similar variable amplitude loading. *Mechanical Systems and Signal Processing* 161: 107856. <https://doi.org/10.1016/j.ymsp.2021.107856>
- Molina, Alejandro, Manuel R. Piña-Monarez, and Jesús M. Barraza-Contreras. 2020. Weibull S-N fatigue strength curve analysis for A572 Gr. 50 steel, based on the true stress-true strain approach. *Applied Sciences (Switzerland)* 10 (16): 1–12. <https://doi.org/10.3390/app10165725>.
- Monedero-Contreras, Ricardo D., Francisca Martínez-Ruiz, and Francisco J. Rodríguez-Tovar. 2023. Evidence of postdepositional remobilization of redox-sensitive metals across sapropel boundaries: New insights from LA-ICP-MS and EDX mapping analyses. *Chemical Geology* 636 (July): 121643. <https://doi.org/10.1016/j.chemgeo.2023.121643>.
- Nagode, Marko, Simon Oman, Jernej Klemenc, and Branislav Panić. 2023. Gumbel mixture modelling for multiple failure data. *Reliability Engineering and System Safety* 230 (October 2022): 108946. <https://doi.org/10.1016/j.res.2022.108946>.
- Nasir, N. N.M., S. Abdullah, S. S.K. Singh, and S. M. Haris. 2020. Risk-based life assessment of prediction models on suspension system for various road profiles. *Engineering Failure Analysis* 114 (April): 104573. <https://doi.org/10.1016/j.engfailanal.2020.104573>.
- Pachapuri, M. Sadiq A., Ravi G. Lingannavar, Nagaraj K. Kelageri, and Kritesh K. Phadate. 2021. Design and analysis of lower control arm of suspension system. *Materials Today: Proceedings* 47 (June 2022): 2949–56. <https://doi.org/10.1016/j.matpr.2021.05.035>.
- Park, Jae Phil, Junhyuk Ham, Subhasish Mohanty, Dayu Fajrul Falaakh, Ji Hyun Kim, and Chi Bum Bahn. 2023. Statistical analysis of S–N type environmental fatigue data of Ni-Base alloy welds using weibull distribution. *Nuclear Engineering and Technology* 55(5): 1924–34. <https://doi.org/10.1016/j.net.2022.08.005>.
- Patil, Sammed, and Sainand Jadhav. 2020. Experimental and FEA of optimized existing lower control ARM. *International Research Journal of Engineering and Technology (Irjet)* 07(07): 5564–5470.
- Pham, Quang Hung, Martin Gagnon, Jérôme Antoni, Antoine Tahan, and Christine Monette. 2021. Rainflow-counting matrix interpolation over different operating conditions for hydroelectric turbine fatigue assessment. *Renewable Energy* 172: 465–76. <https://doi.org/10.1016/j.renene.2021.03.036>.
- Ptak, Michal, and Jerzy Czmochoowski. 2023. Using computer techniques for vibration damage estimation under stochastic loading using the monte carlo method for aerospace applications. *Probabilistic Engineering Mechanics* 72 (March): 103452. <https://doi.org/10.1016/j.probengmech.2023.103452>.
- Putra, T. E., S. Abdullah, and D. Schramm. 2020. Effect of cycle amplitude removal of fatigue strain loadings associated to signal energy characteristics. *Engineering Failure Analysis* 116 (July): 104723. <https://doi.org/10.1016/j.engfailanal.2020.104723>.
- Putra, T. E., Husaini, and M. Ikbali. 2021. Automotive suspension component behaviors driven on flat and rough road surfaces. *Heliyon* 7 (7): e07528. <https://doi.org/10.1016/j.heliyon.2021.e07528>.
- Putra, T. E., Husaini, and M. N. Machmud. 2020. Predicting the fatigue life of an automotive coil spring considering road surface roughness. *Engineering Failure Analysis* 116: 104722. <https://doi.org/10.1016/j.engfailanal.2020.104722>.
- Rahim, A. A.A., S. Abdullah, S. S.K. Singh, and M. Z. Nuawi. 2021. Fatigue strain signal reconstruction technique based on selected wavelet decomposition levels of an automobile coil spring. *Engineering Failure Analysis* 125 (January): 105434. <https://doi.org/10.1016/j.engfailanal.2021.105434>.
- Sarkar, Arnab, Sneha Deep, D. Datta, Amit Vijaywargiya, R. Roy, and V. S. Phanikanth. 2019. Weibull and generalized extreme value distributions for wind speed data analysis of some locations in India. *KSCE Journal of Civil Engineering* 23 (8): 3476–92. <https://doi.org/10.1007/s12205-019-1538-4>.
- Singh, S. S.K., S. Abdullah, and A. K. Ariffin. 2020. Fatigue reliability assessment in time domain using stochastic-induced random stress loads due to limited experimental data. *Engineering Failure*

- Analysis* 117 (March). <https://doi.org/10.1016/j.engfailanal.2020.104794>.
- Soares, H., V. Anes, M. Freitas, and L. Reis. 2018. Fatigue life of a railway wheel under uniaxial and multiaxial loadings. *Procedia Structural Integrity* 13: 1786–91. <https://doi.org/10.106/j.prostr.2018.12.362>.
- Souiyah, Miloud. 2021. Finite element analyses of automobile crankshaft using ANSYS. *Journal of Engineering Research and Reports* 20 (1): 149–58. <https://doi.org/10.9734/jerr/2021/v20i117258>.
- Strzelecki, Przemysław. 2021. Determination of fatigue life for low probability of failure for different stress levels using 3-parameter weibull distribution. *International Journal of Fatigue* 145 (September 2020). <https://doi.org/10.1016/j.ijfatigue.2020.106080>.
- Tognan, Alessandro, and Enrico Salvati. 2023. Probabilistic defect-based modelling of fatigue strength for incomplete datasets assisted by literature data. *International Journal of Fatigue* 173 (April): 107665. <https://doi.org/10.1016/j.ijfatigue.2023.107665>.
- Tsai, Li Wei, and Alice Alipour. 2020. Assessment of fatigue life and reliability of high-mast luminaire structures. *Journal of Constructional Steel Research* 170: 106066. <https://doi.org/10.1016/j.jcsr.2020.106066>.
- Wang, B. J., Q. Li, Z. S. Ren, and S. G. Sun. 2020. Improving the fatigue reliability of metro vehicle bogie frame based on load spectrum. *International Journal of Fatigue* 132. <https://doi.org/10.1016/j.ijfatigue.2019.105389>.
- Wang, Haijie, Fuzhen Xuan, and Xintian Liu. 2021. Prediction and evaluation of fatigue life under random load based on low load strengthening characteristic. *International Journal of Fatigue* 151 (May): 106346. <https://doi.org/10.1016/j.ijfatigue.2021.106346>.
- Wang, Qiushi, Jinsong Zhou, Dao Gong, Tengfei Wang, and Yu Sun. 2021. Fatigue life assessment method of bogie frame with time-domain extrapolation for dynamic stress based on extreme value theory. *Mechanical Systems and Signal Processing* 159: 107829. <https://doi.org/10.1016/j.ymsp.2021.107829>.
- Welch-Phillips, Adanna, Denys Gibbons, Daniel P. Ahern, and Joseph S. Butler. 2020. What is finite element analysis? *Clinical Spine Surgery* 33 (8): 323–24. <https://doi.org/10.1097/BSD.0000000000001050>.
- Zang, R., B. Xu, D. V. Bompá, V. WY Tam, N. Garcia-Troncoso, and Jianli Hao. 2024. Probabilistic fatigue modelling of concrete materials incorporating recycled tyre rubber under flexural loadings. *Construction and Building Materials* 435 (May). <https://doi.org/10.1016/j.conbuildmat.2024.136862>.
- Zhang, Yi, Yong Lv, and Mao Ge. 2021. Time–frequency analysis via complementary ensemble adaptive local iterative filtering and enhanced maximum correlation kurtosis deconvolution for wind turbine fault diagnosis. *Energy Reports* 7: 2418–35. <https://doi.org/10.1016/j.egyr.2021.04.045>